Air-stable, defectless and magnetoresistance properties in nickel-catalyzed transfer-free graphene

Bo-Yu Chen[1, 2], Bo-Wei Chen[1], Wu-Yih Uen[1], Chi Chen[3], Chiashain Chuang[1, 4, *], Dung-Sheng Tsai[1, 4, *]

[1] Department of Electronic Engineering, Chung Yuan Christian University, Taoyuan, 32023, Taiwan

[2] Department of Physics, National Taiwan University, Taipei, 10617, Taiwan

[3] Research Center for Applied Science, Academia Sinica, Taipei, 11529, Taiwan

[4] Research Center for Semiconductor Materials and Advanced Optics, Chung Yuan Christian University, Taoyuan, 32023, Taiwan

*Authors to whom correspondence should be addressed:chiashain@cycu.edu.tw and dungsheng@cycu.edu.tw

Abstract

A transfer-free graphene with high magnetoresistance (MR) and air stability has been synthesized using nickel-catalyzed atmospheric pressure chemical vapor deposition (APCVD). The Raman spectrum and Raman mapping reveal the monolayer structure of the transfer-free graphene, which has low defects, high uniformity, and high coverage (> 90 %). The temperature-dependent (from 5 K to 300 K) current-voltage (*I*-*V*) and resistance measurements are performed, showing the semiconductor properties of the transfer-free graphene. Moreover, the MR of the transfer-free graphene has been measured over a wide temperature range (5-300 K) under a magnetic field of 0 to 1T. As a result of the Lorentz force dominating above 30 K, the transfer-free graphene exhibits positive MR values, reaching ~8.7% at 300 K under a magnetic field (1 Tesla). On the other hand, MR values are negative below 30 K due to the predominance of the weak localization (WL) effect. Furthermore, the temperature-dependent MR values of transfer-free graphene are almost identical with and without a vacuum annealing process, indicating that there are low defects and impurities after graphene fabrication processes so as to apply in air-stable sensor applications. This study opens avenues to develop 2D nanomaterial-based sensors for commercial applications in future devices.

1. Introduction

Graphene, the first two-dimensional (2D) material, attracted a lot of attention in the field of material science and condensed matter physics owing to its ultrathin geometry, high carrier mobility [1], excellent thermal conductivity [2-4], and high mechanical strength [5-7]. Until now, various graphene-based devices have already displayed superior magnetoresistance (MR) characteristics and the related mechanism has been investigated over the years. For instance, the exfoliated graphene nanoribbon-field effect transistor (FET) devices showed a giant magnetoresistance (~100% at 1.6 K and ~50% at 300 K under a high magnetic field (B) of 8 T), resulting from the reduction of backscattering at edge roughness by the delocalization effect at a high magnetic field [8]. Furthermore, the giant MR of ~400 % (at 1.9 K) and ~275% (at 300 K) were observed in single-layer exfoliated graphene with an applied field of 9 T due to the inhomogeneous charge distribution resulting from charged impurities [9]. On the other hand, large-area disordered chemical vapor deposition (CVD) graphene also reveals nice magnetoresistance in shunted CVD graphene with MR of ~600 % under B = 12 T (at 4.2 K) [10] and in a top hexagonal boron nitride (h-BN) capping layer CVD graphene with non-saturating MR of ~140 % under B = 9 T (at room temperature) [11]. Moreover, classical and quantum linear magnetoresistance transport behaviors also were performed in disordered epitaxial graphene systems [12-14] and defect-induced and doping graphene foam systems [15-18].

Nevertheless, several drawbacks need to be overcome before employing graphene as storage devices for practical applications. The first limitation is that a huge operation magnetic field (over 8 T) is required for these graphene devices, making the low-cost target difficult to achieve. The second limitation is the lack of a large-scale and highly uniform directly grown graphene on insulating substrates by chemical vapor deposition (CVD), which will induce unwanted defects and residues of graphene layers and could cause structural changes and distortions in the graphene films during the transfer processes [19]. These drawbacks hinder the development of commercial storage devices by using graphene. On the other hand, graphene grown directly by CVD does not require transfer processes, which is a simple and affordable method as well as compatible with traditional Si fabrication processes [19]. Moreover, compared to other graphene synthesis methods, CVD is regarded as the most crucial method for synthesizing wafer-scale graphene with high uniformity and low defects, as well as a controlled layer number and morphology [20]. To date, copper-catalyzed CVD has been used to synthesize single-layer graphene directly on wafer-scale SiO_2 [21]. However, in contrast to nickel-catalyzed methods [22], this method may be difficult to obtain highly uniform films due to the lower carbon solubility and easily contaminate the CVD system because of the evaporated Ni [23, 24]. Although previous nickel-catalyzed CVD growing methods [25, 26] can yield transfer-free amorphous and defected graphene film on insulating substrates, each of them should be improved further for industrial magnetic sensor applications due to the absence of a wafer-scale, air-stable, defectless and highly uniform single-layer graphene. To the best of our knowledge, nickel-catalyzed CVD growing transfer-free single-layer graphene has not been studied in magnetoresistance transport behaviors. However, the magnetoresistance transport behaviors of transfer-free amorphous carbon thin films growing directly on SiO_2 have been reported and showed the interesting angular dependent MR from low temperature to room temperature due to the sp^2 carbon bonding of graphene-like

honeycomb structure [27, 28], suggesting the great potential of MR in transfer-free single-layer graphene films, which make them suitable for applications in low-cost the magnetic storage devices.

In this study, the synthesis of nickel-catalyzed transfer-free single-layer graphene with high MR was achieved by APCVD. Based on Raman spectra and mapping (10 × 10 μm), transfer-free graphene has a high single-layer coverage (over 90 %), low defects, and high uniformity. A temperature-dependent current and voltage (*I*-*V*) and resistance measurements were conducted on transfer-free single-layer graphene, revealing its semiconductor properties. It exhibited positive MR values above 30 K owing to Lorentz force dominating, reaching 8.7% under a 1 T magnetic field at 300 K. Below 30 K, WL effects prevail, resulting in negative MR values. The transfer-free single-layer graphene, whether annealed in the vacuum or not, also shows almost identical temperature-dependent MR values, suggesting that low defects and impurities remain after the synthesis processes of graphene so as to suitably apply in air-stable sensors. The results of this study provide a foundation for developing large-area graphene-based ultra-thin magnetic sensors and future magneto-transport device applications.

2. Experiment

As shown in Figure 1, a 150-nm nickel film was firstly sputtered on a 100 nm thick SiO_2 substrate (~ 1 cm^2). Ni/SiO_2 substrates were rapidly heated to 600 °C in an APCVD system with a steady Ar flow (purity 99.99%) and held at this temperature for five minutes to enlarge polycrystalline Ni grains, forming an ideal substrate for graphene growth. In the following step, the temperature was increased to 900 °C, and then H_2 flowed for one minute. After that, a graphene growth process was conducted at 900 °C using a flow of hydrogen and methane mixtures in fixed flow rates (75:75 sccm) for three minutes. The grown samples were returned to room temperature after one hour of cooling. After APCVD processes, the uniform transfer-free graphene under the Ni metal surface due to the carbon diffusion [29] could be obtained on the SiO_2 by etching Ni metal films so as to destroy the flowing graphene on the top surface of the Ni metal films in the acid solution (H_2SO_4: HNO_3: CH_3COOH with a volume ratio of 2: 5: 5). A home-built Micro-Raman system conducted Raman measurements with a 532 nm laser excitation source. Temperature-dependent (from 5 K to 350 K) MR of the transfer-free graphene was performed by the Van der Pauw method with standard a.c. voltage lock-in techniques under various magnetic fields (from -1 T to 1T).

3. Results and discussion

In order to provide evidence for high quality and low layer numbers of the transfer-free graphene without damaging our film, we conduct Raman characterization as a nondestructive measuring tool firstly. In the interpretation of the Raman spectrum, the peak around 1582 cm^{-1} (G mode) is caused by a Raman-active E_{2g} phonon (in-plane optical mode) [30]. The D peak (also known as a defect band or a disorder band) at 1350 cm^{-1} is caused by breathing modes in sp^2 atoms and activated by defects or graphene edges [30, 31]. The 2D peak (~2700 cm^{-1}) is the second order of the D peak, resulting from a two-phonon lattice vibrational process. Even in graphene without a D peak, the 2D peak always exists since it does not need to be induced by defects [30, 31]. Then the intensity ratio of the 2D peak to the G peak (I_{2D}/I_G) as well as the full width at half maximum (FWHM) of the 2D peak can be used to determine the number of graphene layers (I_{2D}/I_G > 1.3 and FWHM < 30 cm^{-1} for a single-layer graphene; I_{2D}/I_G < 0.7 and FWHM > 70 cm^{-1} for a multi-layer graphene) [30-34]. As shown in Figure 2 (a), the characterization results (I_{2D}/I_G ratio

value~1.4 and the FWHM of the 2D peak ~28 cm^{-1}) correspond to the features of single-layer graphene. In addition, the weak D peak indicates that our transfer-free CVD processes just introduce few defects into the graphene layer. To evaluate graphene uniformity across a surface, a two-dimensional Raman mapping measurement is performed. As shown in Figure 2 (b), the Raman mapping for the transfer-free CVD graphene exhibits the I_{2D}/I_G ratio value at each sampling point (sampling step: 0.6 μm) over a 10 μm × 10 μm region. Since over 90 % of the I_{2D}/I_G ratio is greater than 1.3, the results indicate that the SiO_2 surface is uniformly covered by monolayer graphene [30, 31].

For the sake of measuring the electrical properties of the transfer-free graphene, the electrical contacts were fabricated by printing conductive silver (Ag) paste, as shown in Figure 3 (a). In Figure 3 (b), the temperature-dependent *I*-*V* curves of transfer-free graphene devices were measured from -20 mV to 20 mV. From the linear *I*-*V* performance, we observe that the semimetal transport of graphene property and Ag contacts are good quality ohmic contacts. In addition, the slope of *I*-*V* curves increases with respect to increasing temperature, which implies the semiconductor properties of the transfer-free graphene due to some defects and impurities within the graphene.

Here we define MR = [R(*B*)-R(0)]/R(0) × (100%), where R(*B*) and R(0) are the resistances at different magnetic fields and at 0 T, respectively [9]. As shown in Figure 3 (c), a positive or negative magnetic field perpendicular to the surface of the transfer-free graphene has been applied to measure the symmetric MR over a wide temperature range (5-300 K). Above 30 K, the transfer-free graphene showed positive MR values owing to the Lorentz force dominant and the maximum positive MR value of 8.7 % occurs at 300 K under a 1 T magnetic field [35, 36]. Compared to the previous study on the MR of single-layer graphene flakes at room temperature [9], the MR value of the transfer-free graphene in this study is competitive due to zero gate bias, weak magnetic field operations and easy fabrication processes. Furthermore, we observe the similar linear MR behavior in graphene at high magnetic fields, which can be understood as a classical limit, where the quantum Hall effect becomes less pronounced. In the low-temperature region, the MR value was negative due to the predominance of the WL effect in the 2D system, which is consistent with low defects and impurities so as to cause disordered properties in our nickel-catalyzed transfer-free monolayer graphene [37, 38]. WL phenomenon is induced while electrons are coherently backscattered along a closed trajectory in disordered two-dimensional systems, which further supports the nickel-catalyzed transfer-free 2D graphene transport properties [34]. Previous reports have shown that elastic electron scattering (such as electron scattering from graphene lattice defects) can induce the WL phenomenon in graphene [35]. Compared to other transferred graphenes (such as exfoliated graphene flake [37, 38], CVD graphene [39] and the epitaxial graphene on the SiC [39, 40]), the WL phenomenon of the transfer-free graphene in this study has been observed for the first time. Therefore, the total MR of the transfer-free graphene can be explicitly expressed as [35]:

$$(MR)_{total} = (MR)_{Lorentz} + (MR)_{WL} \qquad (1)$$

, where $(MR)_{Lorentz}$ is positive MR resulting from Lorentz force, and $(MR)_{WL}$ is negative MR induced by the WL phenomenon. The total MR values above 30 K will be dominated by $(MR)_{Lorentz}$, while values below 30 K will be dominated by $(MR)_{WL}$. Figure 4 implies the result while the resistance decreases with respect to the increasing temperature, which can be explained by the disordered transport properties due to low defects, impurities and grain boundaries of CVD single-layer graphene [40]. As the temperature

rises, phase-breaking processes become more dominating due to thermal energy, which reduces these quantum interference effects, thus lowering the resistance contribution from weak localization.

In addition, due to the large limitation of defect and impurity, the mobility of the transfer-free graphene at room temperature could be further obtained [35]:

$$(MR)_{Lorentz} \approx 1/2\ (\mu \times B)^2 \qquad (2)$$

, where μ is the mobility and B is the magnetic field. The calculated mobility of the transfer-free graphene at room temperature is about 4170 cm^2/Vs. To compare with the mobility of conventional CVD single-layer graphene (from 1000 cm^2 /Vs to 10000 cm^2 /Vs) [42, 43], the mobility of our transfer-free graphene should be further improved via reducing the defects and impurity as well as increasing the single crystal domain for increasing the MR value.

In general, the electrical properties of graphene could be influenced by air absorptions (such as oxygen and water molecules) due to defects and impurities [44]. In order to explore defects and impurities situations within our nickel-catalyzed transfer-free graphene, we performed the transfer-free graphene with/without vacuum annealing method [44] (at 375 K in one minute) processes in our vacuum chamber ($P \sim 10^{-6}$ Torr) and cool down to measure the magnetoresistances under different magnetic fields, as shown in Figure 5 (a) - 5 (c). Temperature-dependent MR values of transfer-free graphene with or without vacuum annealing processes are almost identical at 0.50 T, 0.75 T, and 1.00 T, indicating that there are low defects and impurities on our nickel-catalyzed transfer-free single-layer graphene that is ideal for air-stable magnetic sensor applications. It is important to note that the transfer-free graphene MR value reaches saturation after 200 K, similar to the behavior observed in high quality mechanically exfoliated graphene flake [9].

4. Conclusion

Our nickel-catalyzed APCVD process was applied to synthesize transfer-free graphene with high MR at room temperature and high air stability. From the Raman spectrum and Raman mapping measurements, it was found that the transfer-free graphene has low defects, high uniformity, and high coverage (> 90 %) properties. *I-V* measurements were performed at temperatures ranging from 5 K to 300 K, suggesting the semiconductor properties of the transfer-free graphene. Also, MR measurements of transfer-free graphene have been taken over a wide range of temperatures (5 - 300 K). Positive MR values in transfer-free graphene are dominated by Lorentz force above 30 K, reaching 8.7 % at 300 K under a weak magnetic field (1T). In contrast, WL effects are predominant below 30 K, resulting in negative MR values. In addition, temperature-dependent MR values of the transfer-free graphene, whether vacuum annealed or unannealed, are almost identical, indicating that the transfer-free graphene defects and impurities are relatively low after graphene synthesis. As a result of this research, commercially viable 2D nanomaterial-based magnetic sensors with air stability are now possible for future storage applications.

Figure captions

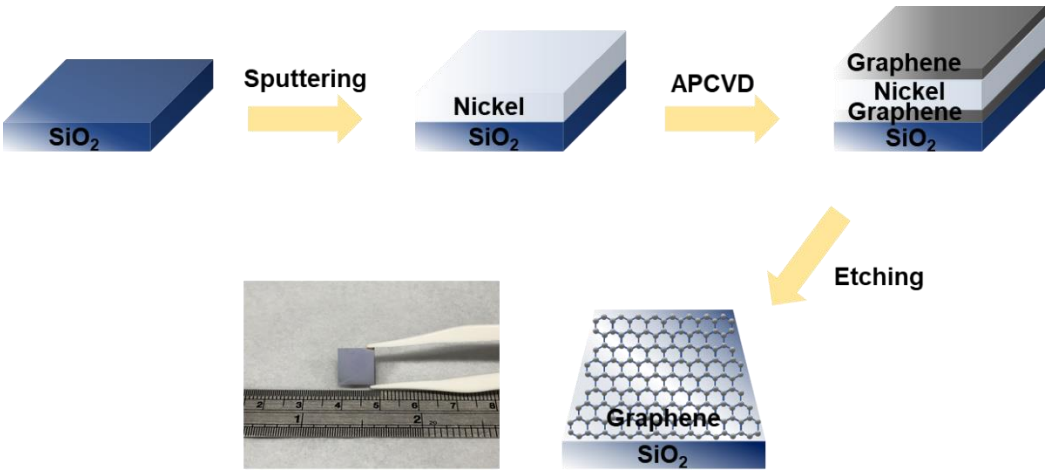

Figure 1. Schematic illustration of the synthesis processes of the transfer-free graphene and a photograph of the transfer-free graphene on SiO_2 (the size of the sample: ~1 cm × 1cm).

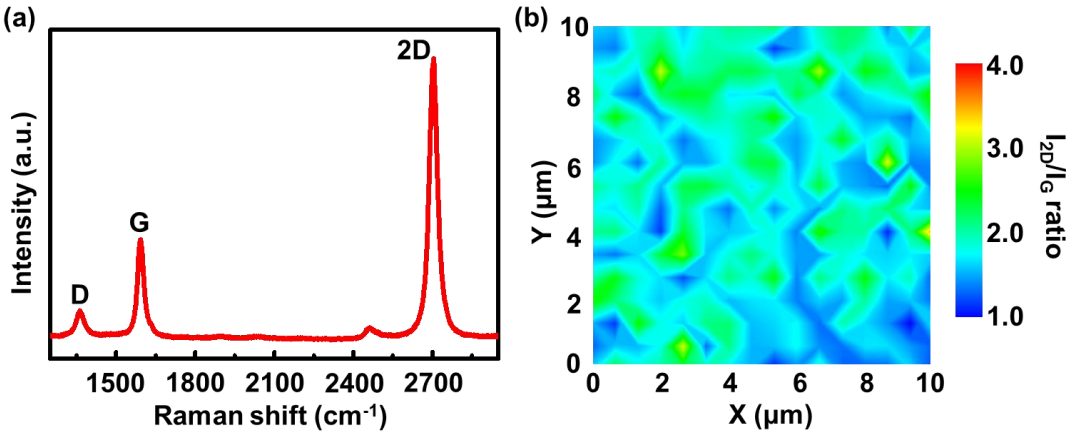

Figure 2. (a) Raman spectrum and (b) I_{2D}/I_G Raman mapping of transfer-free graphene on a SiO_2 substrate (excitation laser: 532 nm).

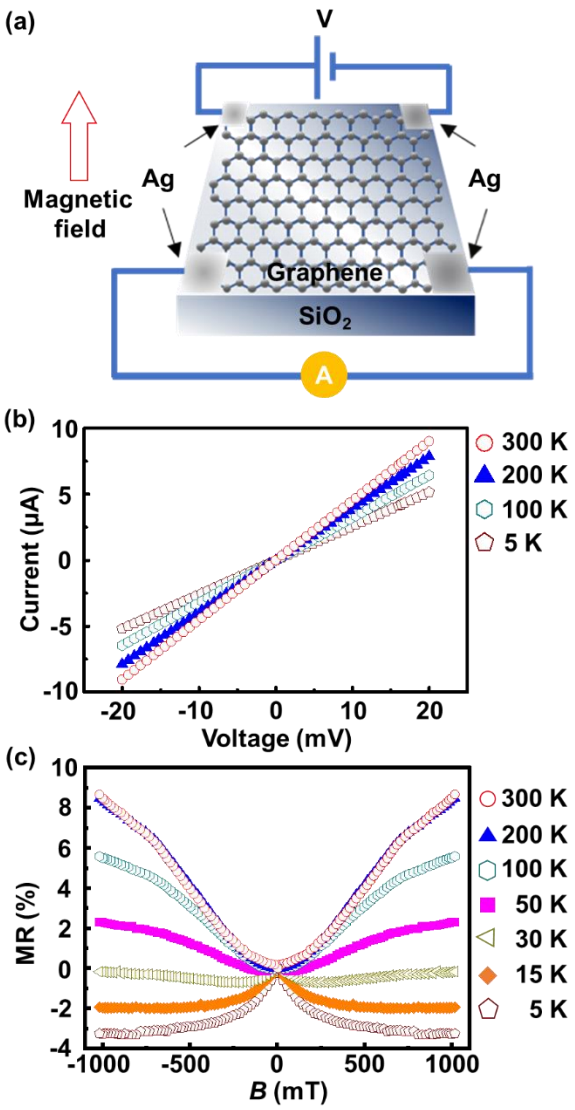

Figure 3. (a) Schematic illustration of transfer-free graphene based devices. (b) *I*–*V* curves of the transfer-free graphene based devices measured at different temperatures. (c) The temperature-dependent symmetric MR value of transfer-free graphene from *B* = -1 T to 1 T.

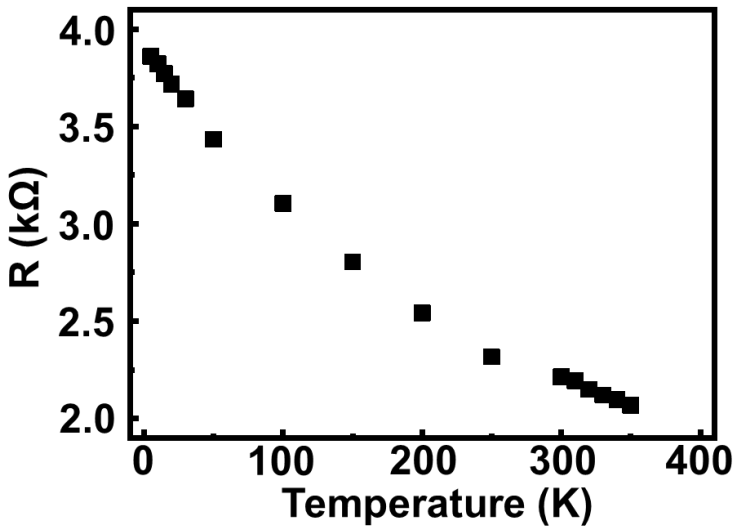

Figure 4. Temperature-dependent resistance of transfer-free graphene.

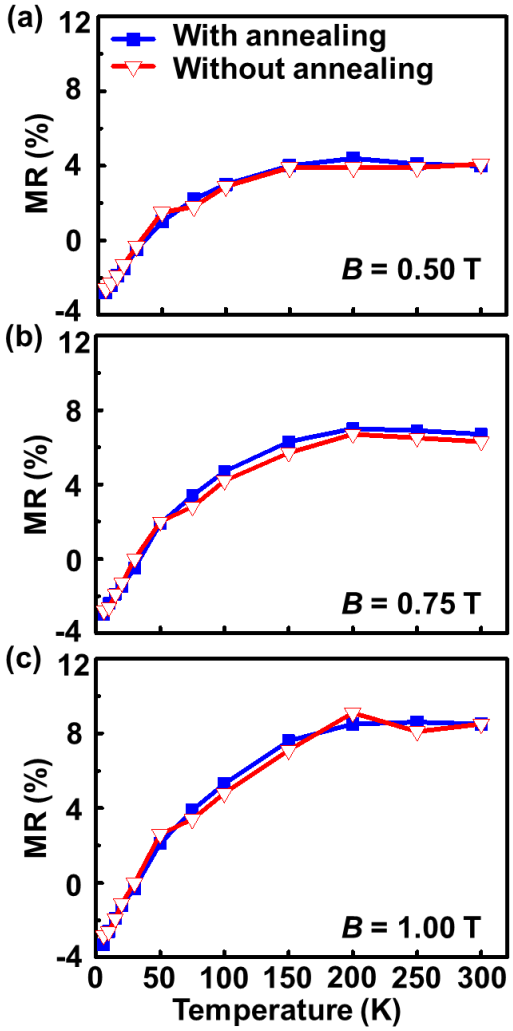

Figure 5. Temperature-dependent MR value of the transfer-free graphene with/without annealing at B = (a) 0.5 (b) 0.75 and (c) 1.00 T.

ACKNOWLEDGMENTS

This work was supported by the National Science and Technology Council, Taiwan, under grant numbers 109-2112-M-033-010-MY3. The authors thank Ms. Shih-Ya Weng (Research Center for Applied Science, Academia Sinica), Mr. Seng Wui Lim (Department of Physics, National Taiwan Normal University) and Prof. Feng Yuh Lo (Department of Physics, National Taiwan Normal University) for their contributions to measure Raman mapping and Raman spectrum of the transfer-free graphene.

References

[1]K. S. Novoselov, A. K. Geim, S. V. Morozov, D.-e. Jiang, Y. Zhang, S. V. Dubonos, I. V. Grigorieva and A. A. Firsov 2004 *Science* 306, 666.

[2] A. A. Balandin 2011 *Nat. Mater.* 10, 569.

[3] A. A. Balandin, S. Ghosh, W. Bao, I. Calizo, D. Teweldebrhan, F. Miao and C. N. Lau 2008 *Nano Lett.* 8, 902.

[4] E. Pop, V. Varshney and A. K. Roy 2012 *MRS Bull.* 37, 1273.

[5] Y. Liu, B. Xie, Z. Zhang, Q. Zheng and Z. Xu 2012 *J. Mech. Phys. Solids.* 60, 591.

[6] I. Frank, D. M. Tanenbaum, A. M. van der Zande and P. L. McEuen 2007 *J Vac Sci Technol B Microelectron Nanometer Struct Process Meas Phenom* 25, 2558.

[7] F. Scarpa, S. Adhikari and A. S. Phani 2009 *Nanotechnology* 20, 065709.

[8] J. Bai, R. Cheng, F. Xiu, L. Liao, M. Wang, A. Shailos, K. L. Wang, Y. Huang and X. Duan 2010 *Nat. Nanotechnol.* 5, 655.

[9] K. Gopinadhan, Y. J. Shin, I. Yudhistira, J. Niu and H. Yang 2013 *Phys. Rev. B* 88, 195429.

[10] A. L. Friedman, J. T. Robinson, F. K. Perkins and P. M. Cambell 2011 *Appl. Phys. Lett.* 99, 022108

[11] C. Chuang, C.-T. Liang, G.-H. Kim, R. E. Elmquist, Y. Yang, Y. P. Hsieh, D. K. Patel, K. Watanabe, T. Taniguchi and N. Aoki 2018 *Carbon* 136, 211

[12] R. S. Singh, X. Wang, W. Chen, Ariando and A. T. S. Wee 2012 *Appl. Phys. Lett* 101, 183105

[13] C. Chuang, Y. Yang, R. E. Elmquist and C.-T. Liang 2016 *Mater. Lett.* 174, 118

[14] A. L. Friedman, J. L. Tedsco, P. M. Cambell, J. C. Culbertson, E. Aifer, F. K. Perkins, R. L. Myers-ward, J. K. Hite, C. R. Eddy, Jr., G. G. Jernigan and D. K. Gaskill 2010 *Nano Lett.* 10, 3962

[15] R. U. R. Sagar, K. Shehzad, A. Ali, F. J. Stadler, Q. Khan, J. Zhao, X. Wang and M. Zhang 2019 *Carbon* 143, 179

[16] Z. Liu, C. Zhen, P. Wang, C. Wu, L. Ma and D. Hou 2019 *Carbon* 148, 512

[17] R. U. R. Sagar, X. Zaiping, J. Iqbal, S. U. Rehman, H. Ashraf, C. Liu, J. Zeng and T. Liang 2021 *Mater. Tod. Phys.* 20, 100460

[18] R. U. R. Sagar, M. Galluzzi, C. Wan, K. Shehzad, S. T. Navale, T. Anwar, R. S. Mane, H.-G. Piao, A. Ali and F. J. Stadler 2017 *ACS Appl. Mater. Interfaces* 9, 1891

[19] C. Chen, D. Dai, G. Chen, J. Yu, K. Nishimura, C.-T. Lin, N. Jiang and Z. Zhan 2015 *Appl. Surf. Sci.* 346, 41.

[20] A. Tzotzis, C. García-Hernández, J.-L. Huertas-Talón, and P. Kyratsis 2020 *Micromachines* 11, 798.

[21] C-Y. Su, A-Y. Lu, C-Y. Wu, Y-T. Li, K-K. Liu, W. Zhang, S-Y. Lin, Z-Y. Juang, Y-L. Zhong, F-R. Chen and L-J Li 2011 *Nano Lett.* 11, 3612-16.

[22] Reina A, Jia X, Ho J, Nezich D, Son H, Bulovic V, Dresselhaus M S and Kong J 2009 *Nano Lett.* 9 30-35
[23] L. Lin, B. Deng, J. Sun, H. Peng and Z. Liu 2018 *Chem. Rev.* 118, 9281–9343.
[24] D. Q. McNerny, B. Viswanath, D. Copic, F. R. Laye, C. Prohoda, A. C. Brieland-Shoultz, E. S. Polsen, N. T. Dee, V. S. Veerasamy and A. J. Hart 2014 *Sci. Rep.* 4, 5049.
[25] J. Kwak, J. H. Chu, J.-K. Choi, S.-D. Park, H. Go, S. Y. Kim, K. Park, S-D. Kim, Y-W. Kim, E. Yoon, S. Kodambaka and S.-Y. Kwon 2012 *Nat. Commun.* 3, 645
[26] Y. Bleu, F. Bourquard, J.-Y. Michalon, Y. Lefkir, S. Reynaud, A.-S. Loir, V. Barnier, F. Garrelie and C. Donnet 2021 *Appl. Surf. Sci* 555, 149492
[27] A. S. Saleemi, A. Abdullah, M. Saeed, M. Anis-ur-Rehman, A. Mahmood, K. Khan, M. Kiani and S.-L. Lee 2019 *Crystals* 9, 124
[28] R. U. R. Sagar, A. S. Saleemi, X. Zhang 2015 *J. Appl. Phys.* 117, 174503
[29] Z. Peng, Z. Yan, Z. Sun and J. M. Tour 2011 *ACS Nano* 5, 8241
[30] A. C. Ferrari, J. C. Meyer, V. Scardaci, C. Casiraghi, M. Lazzeri, F. Mauri, S. Piscanec, D. Jiang, K. S. Novoselov, S. Roth and A. K. Geim 2006 *Phys. Rev. Lett.* 97, 187401.
[31] A. C. Ferrari 2007 *Solid State Commun.* 143, 47.
[32] D. Graf, F. Molitor, K. Ensslin, C. Stampfer, A. Jungen, C. Hierold and L. Wirtz 2007 *Nano Lett.* 7, 238.
[33] P. Zhao, S. Kim, X. Chen, E. Einarsson, M. Wang, Y. Song, H. Wang, S. Chiashi, R. Xiang and S. Maruyama 2014 *ACS Nano* 8, 11631.
[34] X. Xu, C. Lin, R. Fu, S. Wang, R. Pan, G. Chen, Q. Shen, C. Liu, X. Guo and Y. Wang 2016 *AIP Adv.* 6, 025026.
[35] V. Bayot, L. Piraux, J.-P. Michenaud and J.-P. Issi 1989 *Phys. Rev. B* 40, 3514.
[36] Y. Sun, M. Zhang, L. Dong, G. Wang, X. Xie, X. Wang, T. Hu and Z. Di 2018 *AIP Adv.* 8, 045214.
[37] S. V. Morozov, K. S. Novoselov, M. Katsnelson, F. Schedin, L. Ponomarenko, D. Jiang and A. K. Geim 2006 *Phys. Rev. Lett.* 97, 016801.
[38] F. Tikhonenko, D. Horsell, R. Gorbachev and A. Savchenko 2008 *Phys. Rev. Lett.*100, 056802.
[39] A. Baker, J. Alexander-Webber, T. Altebaeumer, T. Janssen, A. Tzalenchuk, S. Lara-Avila, S. Kubatkin, R. Yakimova, C.-T. Lin and L.-J. Li 2012 *Phys. Rev. B* 86, 235441.
[40] X. Wu, X. Li, Z. Song, C. Berger and W. A. de Heer 2007 *Phys. Rev. Lett.* 98, 136801.
[41] C. Chuang, M. Matsunaga, F.-H. Liu, T.-P. Woo, N. Aoki, L.-H. Lin, B.-Y. Wu, Y. Ochiai and C.-T. Liang 2016 *Nanotech.* 27, 075601
[42] A. Venugopal, J. Chan, X. Li, C. W. Magnuson, W. P. Kirk, L. Colombo, R. S. Ruoff and E. M. Vogel 2011 *J. Appl. Phys.* 109, 104511.
[43] D. De Fazio, D. G. Purdie, A. K. Ott, P. Braeuninger-Weimer, T. Khodkov, S. Goossens, T. Taniguchi, K. Watanabe, P. Livreri and F. H. Koppens 2019 *ACS nano* 13, 8926.
[44] C. Chuang, Y. Yang, S. Pookpanratana, C. A. Hacker, C.-T. Liang and R. E. Elmauist, 2017 Nanoscale 9, 11537